Current Optics and Photonics
Vol. 4, No. 4, August 2020, pp. 330-335

ISSN: 2508-7266(Print) / ISSN: 2508-7274(Online)
DOI: https://doi.org/10.3807/COPP.2020.4.4.330

Optimized Working Distance of a Micro-optic OCT Imaging Probe

Da-Seul Kim and Sucbei Moon*

Department of Physics, Kookmin University, Seoul 02707, Korea

(Received March 4, 2020 : revised May 20, 2020 : accepted May 21, 2020)

We have investigated optimization of the working distance (WD) for a highly miniaturized imaging probe for endoscopic optical coherence tomography (OCT). The WD is the axial distance from the distal end of the imaging probe to its beam focus, which is demanded for dimensional margins of protective structures, operational safety, or full utilization of the axial imaging range of OCT. With an objective lens smaller than a few hundred micrometers in diameter, a micro-optic imaging probe naturally exhibits a very short WD due to the down-scaled optical structure. For a maximized WD careful design is required with the optical aperture of the objective lens optimally filled by the incident beam. The diffraction-involved effect was taken into account in our analysis of the apertured beam. In this study, we developed a simple design formula on the maximum achievable WD based on our diffraction simulation. It was found that the maximum WD is proportional to the aperture size squared. In experiment, we designed and fabricated very compact OCT probes with long WDs. Our 165-μm-thick fiber-optic probes provided WDs of 3 mm or longer with reasonable OCT imaging performance.

Keywords : Optical coherence tomography (OCT), Endoscopic optical coherence tomography (OCT), Lens system design

OCIS codes : (110.4500) Optical coherence tomography; (170.2150) Endoscopic imaging; (220.3620) Lens system design; (230.3990) Micro-optical devices

I. INTRODUCTION

The endoscopic techniques of optical coherence tomography (OCT) and other imaging modalities have been rigorously researched for minimally invasive medical imaging based on highly miniaturized imaging probes of catheter and needle forms [1, 2]. The size of very compact OCT imaging probes ranges from 0.1 mm in diameter fabricated with graded-index (GRIN) optics, ball-shaped lensed fibers, or lens-less configuration [1-6]. In endoscopic OCT imaging, such micro-optic probes can be inserted more deeply into the targeted imaging areas with minimal concern. They can also be more easily integrated with conventional instruments owing to the small sizes [7, 8]. There are growing interest and demand for compact endoscopic solutions in various applications of OCT and other imaging modalities.

Ultimate miniaturization of optical assemblies inevitably brings performance limitations involving technical difficulties of optical design and the fundamental limits of micro-optics [5, 9, 10]. One of the most common and critical problems is concerned with the optical performance of the working distance (WD). As a convention, the WD is defined by the distance of the beam's focus on the object side from the structural end of the imaging probe. It provides a dimensional margin for the main imaging region located in the vicinity of the focal point. The WD unavoidably decreases as the optical elements are scaled down in micro-optic devices. However, a certain level of WD is often necessary for small imaging probes operated with protective structures such as tubings or windows. Some applications may require sufficient WDs simply for safe operation. Particularly in OCT imaging, the axial imaging range available is restricted by a very short WD. For the very compact OCT imaging probes thinner than 200 μm in the literature, the WDs were mostly shorter than 1 mm. This level of WD might not provide sufficient dimensional

*Corresponding author: moons@kookmin.ac.kr, ORCID 0000-0002-6742-0937

Color versions of one or more of the figures in this paper are available online.

margins and it might limit the applicability of highly miniaturized OCT probes in some cases.

In this study, we have systematically investigated how to optimize WD performance for a very compact OCT imaging probe. The questions of interest are what the optimal mode of the optical beam filling is, and how long the maximized WD can be for given requirements of focal beam size and lens size. In our study, the WD performance was analyzed by diffraction simulation for apertured Gaussian beams. We were able to develop a simple design formula that easily estimates the maximum achievable WD as a useful design guide. Our theoretical analysis was validated by experimental results with our fabricated micro-optic imaging probes. Our analysis and findings on the WD performance will provide a useful design guide for developing structurally compact but optically far-reaching OCT imaging probes.

II. THEORETICAL ANALYSIS

Since single-mode (SM) fiber mostly produces a nearly Gaussian beam at its output, extensive studies have been carried out for the beam-focusing optics of OCT imaging probes based on the Gaussian beam model [11], in which the beam is not spatially restricted by the lens aperture. The Gaussian beam parameters and the lens transfer matrix, better known as the ABCD matrix, provide a simple formalism for performance estimation. In practice, the beam-aperturing effect limits the WD achieved with a real-world lens of definite size. For a demanded focal beam size which constrains the object-side numerical aperture (NA), a small lens cannot provide a large aperture and a long WD at the same time. A Gaussian beam of wavelength λ and focal beam size w_0 gives a beam divergence angle of $\lambda/(\pi w_0)$ out of its focal region. In approximation, a low-NA lens of diameter D is desirably underfilled only if the WD is as short as

$$\mathrm{WD} < \frac{\pi D w_0}{2\lambda}, \tag{1}$$

for the beam to be still effectively Gaussian. Otherwise, the beam is spatially filtered in the beam overfilling, and prone to aperture-induced diffraction. This brief analysis suggests that the maximum achievable WD depends upon the lens size and the demanded focal beam size. And the simple Gaussian beam model fails in successfully estimating the beam focusing performance. The actual WD limit can be estimated only by formally taking the diffraction effect into account.

An OCT imaging probe that equips a micro-optic objective lens can be modeled by scalar diffraction theory. In our diffraction model, the optical beam fed to the objective is a Gaussian beam produced by SM fiber. This beam is refocused by an objective lens of circular aperture determined by the lens diameter. The beam at the exit plane of the lens, called S, becomes an apertured Gaussian beam with a curved wavefront in spatial phase modulation. Its field on S, denoted by $E_S(u,v)$ in the Cartesian coordinate variables of u and v, is given by

$$E_S(u,v) = E_0 \exp\left[\frac{-r^2}{w_S^2} - ik\left(\frac{r^2}{2R_c}\right)\right]\cdot U(r - R_a), \tag{2}$$

where r is the radial distance defined by the square root of u^2+v^2, w_S is the initial beam size on S in the Gaussian measure, $k = 2\pi/\lambda$ is the radial wavenumber, R_c is the curvature radius of the wavefront or the phase modulation constant, R_a is the aperture radius, and E_0 is an amplitude constant. Here, $U(\zeta)$ is the aperture step function, equal to 1 for $\zeta \le 0$ and 0 for $\zeta > 0$. In the thin-lens case, R_a automatically equals half of the lens diameter, D.

The apertured Gaussian beam of E_S propagates in diffraction after the lens. By the well-known Huygens-Fresnel formula, the diffracted field of E_{dif} is obtained by the surface integral on S as

$$E_{diff}(x,y,z) = \frac{1}{i\lambda}\iint_S E_S(u,v)\cdot\frac{\exp(ikq)}{q}\,dudv, \tag{3}$$

where x and y are the Cartesian coordinate variables of the lateral plane of observation, and z is the axial variable. The illumination plane of S is expressed by $z = 0$. Here, q is the geometrical distance to a point on S, obtained by the square root of $(x-u)^2+(y-v)^2+z^2$. Figure 1 shows a graphical illustration of our model. As a relative measure of the initial beam size, the beam filling factor of F is defined by $F = w_S/R_a$. The condition of overfilled or underfilled launch to the lens is roughly discriminated by the matched-launch condition of $F = 100\%$ with $w_S = R_a$. When overfilled ($F > 100\%$), a considerable portion of the optical power is lost by spatial filtering. For an apertured

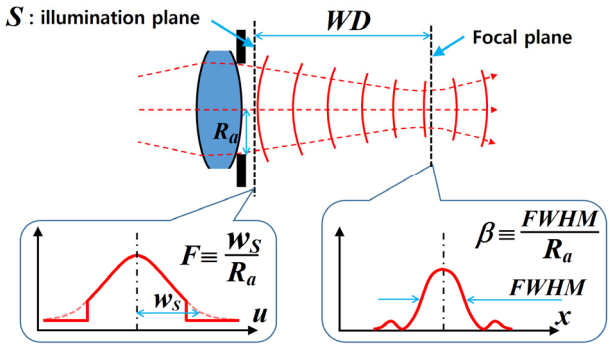

FIG. 1. Diffraction of the apertured Gaussian beam. The beam filling factor, F, relatively measures the beam size at the lens input while β measures the relative size of the focal beam in regard to the aperture size, R_a.

Gaussian beam defined by R_a, F, and R_c, the focal point is found by the smallest beam size of E_{dif}. And the WD is determined by its axial position. The beam size at the focal plane is evaluated by the full width at half maximum (FWHM) of the intensity profile. It is measured relatively by β, which is the FWHM normalized by R_a.

From Eqs. (2) and (3), computational searching for WDs was carried out by our MATLAB code for a working wavelength of $\lambda = 1.3$ μm. Figure 2 shows the calculated WDs and the focal beam sizes obtained with $R_a = 70$ μm for varying R_c. Four different beam-launch conditions were tested with $F = 50\%$, 75%, 100%, and 200%. In the surely underfilled launch of $F = 50\%$, we found that the nearly Gaussian beam exhibits a peak in WD at a certain curvature of R_c. In the other cases of $F = 75\%$, 100%, and 200% where the aperture effect is not negligible, the focal beam size steadily increases with the wavefront curvature until the beam becomes divergent without any focusing behavior. There, the maximum in WD can be technically determined at the focus-vanishing point. Those maximum WDs are marked by colored circles in Figs. 2(a) and 2(b). Notice that the initial beam size is quantified by w_S in the Gaussian measurement, which is the beam radius of intensity e^{-2}. The FWHM beam size can be estimated as $1.18 \times w_S$ for the Gaussian beam.

For the apertured Gaussian beams of $F = 75\%$, 100%, and 200%, growth of the WD is accompanied by increase of the focal beam size. A practical maximum in WD should be determined in regard to the focal beam size. For instance, if the focal beam size is required to be below 50 μm, the maximum achievable WD is found to be 3.3 mm, 3.5 mm, and 3.9 mm for the three cases of $F = 75\%$, 100%, and 200%, respectively. It is obvious that a higher value of F gives a longer WD as expected. However, the increment is not so high. This comes from the fact that the curves for WD shown in Fig. 2(a) follow the same trend, despite the different filling factors, and those for the focal beam sizes are dispersed very little, as observed in Fig. 2(b). Therefore, excessive filling or increasing F is not a power-effective strategy for practically maximizing the WD. An optimal level for F was found to be around 100%. Further increase of F provides a slightly enhanced WD, but with an excessive optical power loss above 13.5% or 0.6 dB. This is a useful finding for optimization of the WD performance.

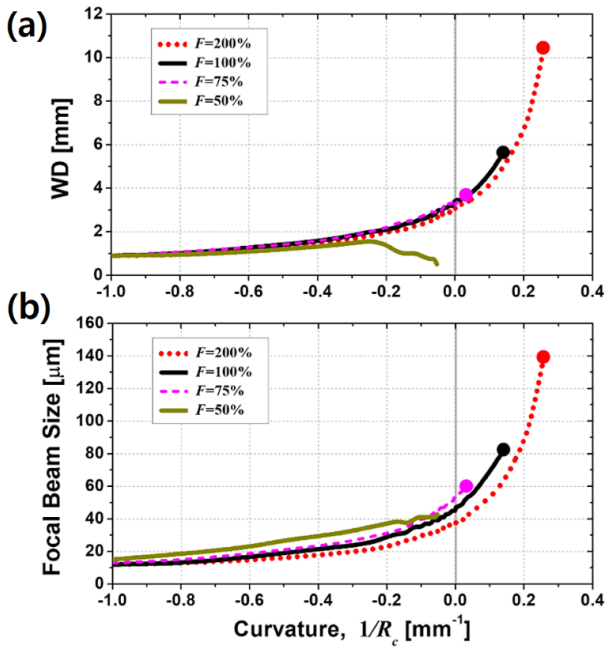

FIG. 2. Increase of the WD (a) and the focal beam size (b) with wavefront curvature, $1/R_c$, theoretically calculated for the four different beam filling factors. Note that the aperture size, R_a, was kept constant in all the cases. The beam filling factor, F, is the ratio of the Gaussian beam width at the lens incidence to the aperture size of R_a.

The maximum achievable WDs were further investigated under the optimal launch condition of $F = 100\%$. The focal beam size was relatively measured by β, *i.e.*, the ratio of the focal beam size in FWHM to the aperture radius R_a. Figure 3 shows the maximum achievable WD for a wide range of R_a calculated for the three cases of $\beta = 0.35$, $\beta = 0.59$, and $\beta = 0.83$. Both the horizontal and vertical axes are normalized by λ for scaling analysis. An empirical formula for the maximum achievable WD was obtained by curve fitting of the simulation results. The curves for the maximum WDs were nicely approximated by parabolas. In the range of $R_a/\lambda = 20$ to 180, the maximum achievable WD is expressed by

$$\frac{\mathrm{WD}_{\max}}{\lambda} \approx a \cdot \left(\frac{R_a}{\lambda}\right)^2, \tag{4}$$

where a is the fit coefficient. Our curve fitting gave $a = 0.52$ for $\beta = 0.35$, $a = 0.83$ for $\beta = 0.59$, and $a = 1.10$ for

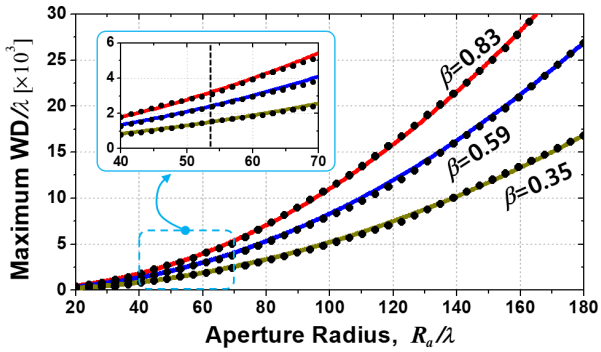

FIG. 3. Maximum achievable WD as a function of aperture radius for three different relative focal beam sizes. Both axis scales are normalized by λ. The dotted curves show the computational results while the solid lines are their parabolic curve fits. The inset gives a magnified view around $R_a/\lambda = 53.8$, marked by the vertical dashed line. Note that the relative focal beam size, β, is the ratio of the FWHM size at the focus to the aperture size, R_a.

$\beta = 0.83$, respectively. One can easily calculate the maximum achievable WD for given values of λ and R_a by using Eq. (4).

The results shown in Fig. 3 and Eq. (4) are scalable for different working wavelengths. In diffraction theory, reduction of the wavelength is equivalent to extension of the structural dimensions. Thus, the same value for the maximum WD normalized by λ is found for a normalized aperture radius of R_a/λ. Eq. (4) suggests that the maximum WD is inversely proportional to the wavelength in the same optical structure. For example, with $R_a = 70$ μm and $\beta = 0.59$ for $F = 100\%$, the maximum WD is found to be 3.1 mm at $\lambda = 1.3$ μm. Reducing λ by half simply doubles the normalized aperture radius, and quadruples the normalized WD. Accordingly, the maximum WD for $\lambda = 0.65$ μm is calculated to be 6.3 mm from Eq. (4).

III. EXPERIMENTAL VALIDATION

We designed and fabricated very compact, long-WD imaging probes in this study. GRIN lens elements were utilized in our micro-optic probes. Our GRIN lenses came originally from custom-fabricated graded-index optical fiber, cleaved and polished carefully for making short GRIN lenses. The full diameter of the fiber was 165 μm including the cladding layer while the real diameter of the GRIN profile was 140 μm, hence, giving approximately $R_a = 70$ μm. Figure 4 shows the schematic diagram of our imaging probe and the microscopic picture of a fabricated probe. The GRIN lens was assembled with standard SM fiber by using a spacing element of coreless silica fiber. All of them were in fiber form and could be fusion-spliced one by one for a compact and robust structure [1]. The free design parameters in our micro-optical assembly were the length of the spacer, L_s, and the length of the GRIN lens, L_g. The lens power was determined by L_g for a given GRIN lens coefficient. The pitch of our GRIN lens was found to be 2.27 mm. The working wavelength was $\lambda = 1.3$ μm.

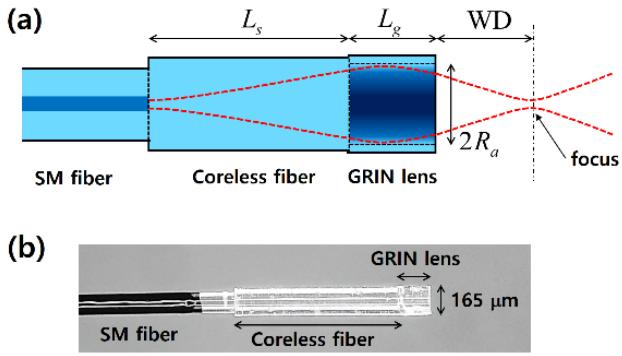

FIG. 4. Schematic diagram of our imaging probe with the design parameters defined (a), and the microscopic view of a fabricated probe (b).

The length of the spacer element, L_s, was carefully chosen at first so that the beam filling factor of F was set to be 100%. We experimentally found the length of L_s for which the beam size immediately after the spacer matched the aperture size of the lens. In the next step, the GRIN-lens fiber was spliced to the spacer. And the GRIN-lens fiber was cleaved at the other end by a fiber cleaver while carefully measuring the length with a microscope-equipped translation stage. Two factors affected our controlled determination of the lens length, L_g.: First, the precision of our cleaving work was not fine enough with an error of ±10 μm. Second, fusion splicing deformed the lens slightly in the fused region. Note that the required precision of L_g was finer than a few microns in making a long WD. Additional polishes were applied to the outer plane of the GRIN lens for fine adjustment of L_g.

It is worth noting that our GRIN lens was not a thin lens. The real aperture stop was located in the middle of the GRIN lens. Due to its finite size, the optical fields that reached the cylindrical boundary of the GRIN part radiated out of the lens. In our experiment, index-matching gel was applied to the cladding to keep the unconfined fields from interfering with our beam characterization. As a consequence of the thin-lens approximation, F could be slightly underestimated in our experiment, and the measured WD could be slightly shortened. Those effects were not so strong, though, because the lens length was no more than 0.2 mm in our probes.

After fabrication of our probes, the WDs and the focal spot sizes were evaluated with an SLD light source and an optical microscope equipped with an IR camera. The lengths of L_s and L_g were carefully measured by microscopic inspection. Table 1 summarizes the results of our probe fabrication and testing. For given parameters of $\lambda = 1.3$ μm, $R_a = 70$ μm, and $F = 100\%$, simply calculated from Eq. (4), the maximum achievable WDs are 2.0 mm, 3.1 mm, and 4.1 mm for relative focal beam sizes of $\beta = 0.35$, 0.59, and 0.83, respectively. The experimentally obtained WDs

TABLE 1. Results of probe fabrication and testing

Probe sample ID	Design parameters		Performance factors	
	L_s (mm)	L_g (mm)	WD (mm)	Focal beam size, FWHM (μm)
A	1.03	0.16	4.2	59.4 ($\beta = 0.85$)
B	1.03	0.16	3.6	51.3
C	1.03	0.17	2.9	35.1 ($\beta = 0.50$)
D	1.03	0.17	2.8	31.8
E	1.03	0.18	2.5	28.5
F	1.03	0.19	2.3	27.4
G	1.03	0.20	2.2	25.7
H	1.03	0.19	1.9	22.3 ($\beta = 0.32$)
I	1.02	0.20	1.6	20.2

shown in Table 1 approximately agreed with the theoretical predictions in the three cases of Samples H, C, and A. Note that their relative focal beam sizes were $\beta = 0.32$, 0.50, and 0.85, respectively, in the experimental results. The performance of the fabricated probes was slightly inferior due to imperfect index profile of the GRIN lens or other phase perturbations [9]. The longest of the WDs obtained in our experiment was 4.2 mm with $\beta = 0.85$ (Sample A). We found it very difficult to successfully obtain a longer WD by simply decreasing L_g. Formation of the focus was very sensitive to the lens length for the loosely focused beam. Very often the focal point could not be reliably determined with asymmetric beam shapes. Unintended curvature of the lens plane might sensitively affect the beam quality. In our fabrication, obtaining a very loose focus of $\beta > 0.9$ was technically challenging for those reasons.

For the apertured Gaussian beams, the diffraction behaviors appeared to be very different from those of simple Gaussian beams. Figure 5 shows the axial evolution of the beam size experimentally observed with our probes of Samples C and Sample H. Unlike for simple Gaussian beams, convergence and divergence of the beams turned out to be very asymmetric. They focused in faster than they focused out. In OCT imaging with Gaussian beams, the axial imaging range is conventionally estimated by a multiple of the confocal parameter or the Rayleigh range, simply calculated from the focal beam size [1]. This simple method of estimation is no longer valid for the apertured Gaussian beams. The real characteristics can be engineered only through diffraction analysis, using the integral formula of Eq. (3) or other numerical schemes such as the beam propagation method (BPM) [9]. It is apparent that our WD-prioritized design does not automatically maximize the axial imaging range of OCT. The axial imaging range was roughly halved in regard to the Gaussian-beam case of the same focal beam size. Still, a long axial range could be attained owing to its loose focus of our WD-prioritized design, compared to those of the conventional resolution-prioritized designs.

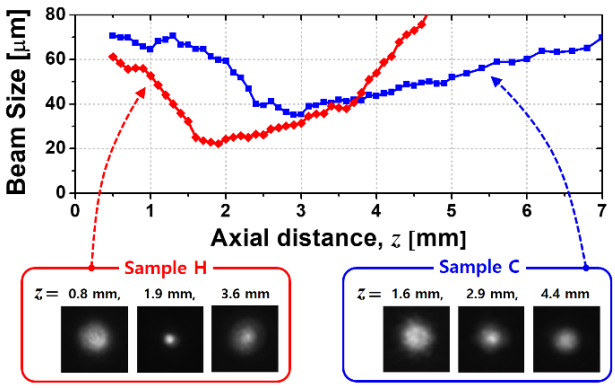

FIG. 5. Axial evolution of beam size (FWHM) for our fabricated probes (Samples C and H), shown together with some of the beam images experimentally acquired.

IV. DISCUSSION

Our formula of Eq. (4) is a useful design guide. One can easily estimate the relation of the achievable WD to the lens size. This enables a WD-prioritized design strategy by which the required WD is defined at first, and then the probe size or the resolution performance is compromised. This must be useful when obtaining a long WD is indispensable. In conventional designs, the focal beam size is first defined for the lateral resolution accepting the resulted WD subject to the lens size. As suggested by Eq. (4), the maximum achievable WD is proportional to the square of the lens size. Obtaining a few millimeters of WD is not so difficult if the lens diameter exceeds 300 μm. However, a micro-optic imaging probe demands careful optimization for an acceptable WD when the lens diameter is thinner than a few hundred micrometers. The WD-prioritized design can be useful in such a case.

As a consequence of its diffractive nature, there is a tradeoff relation between lateral resolution and imaging WD in OCT imaging. A longer WD is achieved by partially sacrificing the lateral resolution. The required level of resolution depends on the type of application. For example, a simple ranging application does not need fine lateral resolution [7]. OCT imaging of layered tissues can still take advantage of high axial resolution, even with a loose beam focus. It is worth noting that fine lateral resolution is only achieved in the vicinity of the focal region with a relatively high NA objective. A maximized WD provides a long imaging range with moderate resolution and an extended depth of focus. Thus, some endoscopic OCT applications may accept or prefer poorer lateral resolution in favor of longer WD or wider axial range of imaging.

To determine the effect of the increased WD and the reduced resolving power, an OCT imaging test was carried out with our fabricated long-WD probe (Sample C). In our imaging test, beam scanning was performed simply by translating the imaging probe. A typical system configuration for swept-source OCT was utilized. Figure 6 shows the obtained OCT images of a human fingertip. In Fig. 6(a) the very long imaging range of our probe is verified,

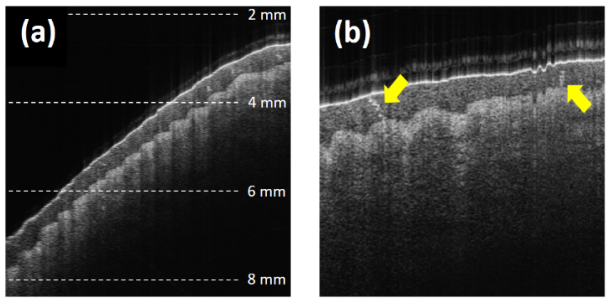

FIG. 6. OCT images of a human fingertip obtained with our imaging probe (Sample C). The sweat glands are marked by the colored arrows.

as depicted by horizontal dashed lines labeled with the axial distances. The image shows reasonable resolution quality, acceptably maintained up to 6 mm. The effective axial range of imaging was estimated to be wider than 4 mm based on the data of Figs. 5 and 6. Locating the tissue under imaging at the focal distance, the best resolution is demonstrated in the OCT image of Fig. 6(b). Marked by the arrows, sweat glands of spiral form were reasonably resolved. The lateral resolution of our probe was 35 μm at best, much lower than those of typical OCT imaging systems by a factor of 2 to 4. However, Fig. 6(b) demonstrates that our probe offers reasonable performance for the case of fingertip imaging. It is still remarkable that a very long WD of 2.9 mm was achieved by a micro-optical structure that was only 165 μm thick.

V. CONCLUSION

In summary, we have investigated the optimization of WD in making a very compact OCT imaging probe. The WD was computationally evaluated by the apertured Gaussian beam model. It has been observed that the diffraction behavior of the apertured beam is quite different from that of a classic Gaussian beam, necessitating diffraction analysis in the probe design. We found that the matched beam filling of $F = 100\%$ is an optimal compromise for a practically maximum WD. For a design guide, we obtained a simple formula for the maximum WD. It was found that the maximum WD is proportional to the square of the lens size. We developed a simple design guide for predicting the practically maximized WD, which will be useful in the future development of highly miniaturized imaging probes with long WDs.

ACKNOWLEDGMENT

This study was supported by a grant from the National Research Foundation of South Korea (NRF-2018R1D1A1B 07045449). We appreciate Mr. Yusi Miao of the University of California, Irvine for helping our OCT imaging.

REFERENCES

1. D. Lorenser, R. A. McLaughlin, and D. D. Sampson, "Optical coherence tomography in a needle format," in *Optical Coherence Tomography: Technology and Applications*, W. Drexler, J. G. Fujimoto, eds. (Springer, 2015), Chapter 81.
2. Z. Yaqoob, J. Wu, E. J. McDowell, X. Heng, and C. Yang, "Methods and application areas of endoscopic optical coherence tomography," J. Biomed. Opt. **11**, 063001 (2006).
3. X. Li, C. Chudoba, T. Ko, C. Pitris, and J. G. Fujimoto, "Imaging needle for optical coherence tomography," Opt. Lett. **25**, 1520-1522 (2000).
4. S. Han, M. V. Sarunic, J. Wu, M. S. Humayun, and C. Yang, "Handheld forward-imaging needle endoscope for ophthalmic optical coherence tomography inspection," J. Biomed. Opt. **13**, 020505 (2008).
5. W. Yuan, R. Brown, W. Mitzner, L. Yarmus, and X. Li, "Super-achromatic monolithic microprobe for ultrahigh-resolution endoscopic optical coherence tomography at 800 nm," Nat. Commun. **8**, 1531 (2017).
6. J. Lee, Y. Chae, Y.-C. Ahn, and S. Moon, "Ultra-thin and flexible endoscopy probe for optical coherence tomography based on stepwise transitional core fiber," Biomed. Opt. Express **6**, 1782-1796 (2015).
7. S. Shin, J. K. Bae, Y. Ahn, H. Kim, G. Choi, Y. S. Yoo, C.-K. Joo, S. Moon, and W. Jung, "Lamellar keratoplasty using position-guided surgical needle and M-mode optical coherence tomography," J. Biomed. Opt. **22**, 125005 (2017).
8. Y. Huang, X. Liu, C. Song, and J. U. Kang, "Motion-compensated hand-held common-path Fourier-domain optical coherence tomography probe for image-guided intervention," Biomed. Opt. Express **3**, 3105-3118 (2012).
9. D. Lorenser, X. Yang, and D. D. Sampson, "Accurate modeling and design of graded-index fiber probes for optical coherence tomography using the beam propagation method," IEEE Photonics J. **5**, 3900015 (2013).
10. L. Scolaro, D. Lorenser, R. A. McLaughlin, B. C. Quirk, R. W. Kirk, and D. D. Sampson, "High-sensitivity anastigmatic imaging needle for optical coherence tomography," Opt. Lett. **37**, 5247-5249 (2012).
11. W. Jung, W. A. Benalcazar, A. Ahmad, U. Sharma, H. Tu, and S. A. Boppart. "Numerical analysis of gradient index lens-based optical coherence tomography imaging probes," J. Biomed. Opt. **15**, 066027 (2010).